JGR Atmospheres

RESEARCH ARTICLE
10.1029/2020JD034080

Special Section:
Atmospheric PM2.5 in China: physics, chemistry, measurements, and modeling

Key Points:

- The particulate fractions of organic molecular markers attained their minima in summer, when the total concentrations increased
- Evaporation loss might be the main sampling artifact of particulate organics when the vapor pressure is lower than 10^{-10} atm
- Total concentrations of organic molecular markers over a wide vapor pressure range should be used for positive matrix factorization analysis

Supporting Information:

Supporting Information may be found in the online version of this article.

Correspondence to:

C. Qin and M. Xie,
chaoqin@njau.edu.cn;
mingjie.xie@nuist.edu.cn;
mingjie.xie@colorado.edu

Citation:

Gou, Y., Qin, C., Liao, H., & Xie, M. (2021). Measurements, gas/particle partitioning, and sources of nonpolar organic molecular markers at a suburban site in the west Yangtze River Delta, China. *Journal of Geophysical Research: Atmospheres*, *126*, e2020JD034080. https://doi.org/10.1029/2020JD034080

Received 12 OCT 2020
Accepted 12 SEP 2021

Author Contributions:

Conceptualization: Chao Qin, Hong Liao, Mingjie Xie
Funding acquisition: Mingjie Xie
Investigation: Yafeng Gou, Chao Qin, Hong Liao
Methodology: Chao Qin, Hong Liao, Mingjie Xie
Project Administration: Mingjie Xie
Supervision: Mingjie Xie

Measurements, Gas/Particle Partitioning, and Sources of Nonpolar Organic Molecular Markers at a Suburban Site in the West Yangtze River Delta, China

Yafeng Gou[1], Chao Qin[2], Hong Liao[1], and Mingjie Xie[1]

[1]Collaborative Innovation Center of Atmospheric Environment and Equipment Technology, Jiangsu Key Laboratory of Atmospheric Environment Monitoring and Pollution Control, School of Environmental Science and Engineering, Nanjing University of Information Science & Technology, Nanjing, China, [2]Colleges of Resources and Environmental Sciences, Nanjing Agricultural University, Nanjing, China

Abstract This study seeks to understand the ambient levels, gas/particle partitioning, and sources of nonpolar organic molecular makers (OMMs) at a suburban site in Nanjing, China. Particle- and gas-phase OMMs were collected using a medium volume sampler equipped with two quartz filters in series and a polyurethane foam (PUF)/XAD-4/PUF (PXP) adsorbent sandwich. More than 100 pairs of filter and PXP samples were collected diurnally from September 2018 to September 2019. The concentration profiles of total *n*-alkanes and polycyclic aromatic hydrocarbons were peaking at *n*-C12–*n*-C17 homologs (9.98 ± 5.43–38.4 ± 17.7 ng m^{-3}) and naphthalene (92.5 ± 56.7 ng m^{-3}), respectively, followed by decreasing concentrations with further increases in molecular weight. Three artifact correction methods with different pre-assumptions on relative contributions of evaporation loss to backup filter measurements were used to separate particle- and gas-phase OMMs. The resulting particle-phase fractions showed significant differences for OMMs with vapor pressure $<10^{-9}$ atm at 298.15 K. Absorptive gas/particle partitioning coefficients of OMMs were empirically calculated based on measurements and theoretically predicted for comparison. The results obtained under the three artifact correction methods suggested growing importance of evaporation loss with decreased vapor pressure. Positive matrix factorization (PMF) was performed for source apportionment using total (PMF_{total}) and particle-phase ($PMF_{particle}$) OMMs data, respectively. Besides eliminating the influence of gas/particle partitioning, the involvements of more volatile species and gaseous OMMs data improved the identification of specific emission sources, supporting the usage of total OMMs data over a wide vapor pressure range for PMF source apportionment.

1. Introduction

Carbonaceous aerosols, composed of organic carbon (OC) and elemental carbon (EC; or black carbon, BC), contribute a significant fraction (20%–50%) of particulate matter with an aerodynamic diameter less than 2.5 μm ($PM_{2.5}$) in polluted atmosphere (Han et al., 2016; Ho et al., 2006; O'Dowd et al., 2002). There is growing evidence that both short- and long-term BC exposure are associated with negative health outcomes (e.g., all cause and cardiovascular mortality) (World Health Organization, 2012), and the short-term effects of EC and OC are greater and more immediate than those of sulfate and nitrate (Kim et al., 2012). BC is the most efficient light absorbent in the atmosphere (Bond et al., 2013), while OC can both scatter and absorb sunlight with inconclusive radiative forcing (Feng et al., 2013; Tuccella et al., 2020; Wang et al., 2014; Yang et al., 2009). Furthermore, the hydrophobic-to-hydrophilic conversion of OC is a potential source of cloud condensation nuclei (Petters et al., 2006). Therefore, an effective source apportionment of carbonaceous aerosols is valuable in developing control measures to reduce their health and climate impacts.

Compositional data of individual organic molecular markers (OMMs) are often used as inputs of receptor models (e.g., chemical mass balance, positive matrix factorization [PMF]) to apportion carbonaceous aerosols to specific emissions sources (Jaeckels et al., 2007; Shrivastava et al., 2007). OMMs have been recognized as better tracers for OC than water soluble elements (Xie et al., 2012), and several $PM_{2.5}$ sources do not have specific elemental compositions (Schauer et al., 1996). However, most OMMs should be regarded as semi-volatile organic compounds (SVOCs), and their gas/particle partitionings are predominately controlled by ambient temperatures (Donahue et al., 2006). To reduce the influence of gas/particle partitioning of OMMs

Writing – original draft: Yafeng Gou, Chao Qin
Writing – review & editing: Chao Qin, Hong Liao, Mingjie Xie

on source apportionment, Xie et al. (2013) suggest using the total concentration data of OMMs, including both gas and particle phases, for PMF modeling. This method has been proven to improve quantifying the source that is characterized by more volatile OMMs and considerable contributions (~20%) to OC and EC in urban Denver (Xie et al., 2014b). In addition, the gas/particle partitioning also affects the lifetime and transport of SVOCs (May et al., 2012; Saleh et al., 2013), as well as the health effect evaluation of toxic compounds. Polycyclic aromatic hydrocarbons (PAHs) are a group of mutagenic and carcinogenic SVOCs, and the potential risk of exposure to particulate PAHs has been exhaustively investigated (Ravindra et al., 2001; Yan et al., 2019). Due to the changes in particle-phase fractions (F%) of PAHs with ambient temperatures, the contribution of gas-phase PAHs to the total carcinogenic risk can vary from ~30% to more than 80% (Ramírez et al., 2011; Wei et al., 2015), which should be taken into account in future risk assessment studies.

To mitigate severe haze pollution events in Chinese cities, power plants were forced to install flue-gas desulfurization and denitrification equipment in 2006 and 2011, respectively. Furthermore, the Air Pollution Prevention and Control Action Plan was issued by the State Council of China in September 2013. This 5-year plan (2013–2017) was targeted to reduce $PM_{2.5}$ concentrations by 15%–25% in the three Chinese megacity clusters—Beijing-Tianjin-Hebei region (Jing-Jin-Ji), Yangtze River Delta (YRD), and the Pearl River Delta (PRD). From 2013 to 2017, the concentrations of $PM_{2.5}$ and its carbonaceous components all showed noticeable downward trends (Wang et al., 2019). Take Nanjing city, a typical mega city located in the west YRD region as an example, the annual average concentration of $PM_{2.5}$ decreased by 46.8% (from 77 to 41 μg m^{-3}; http://hbj.nanjing.gov.cn/); average OC and EC concentrations in urban areas were 18.0 and 6.67 μg m^{-3} in 2013 (Li et al., 2016), and were 5.92 and 2.95 μg m^{-3} in 2017 (Yu et al., 2020); BC exhibited an annual decrease rate of 8.4% at a suburban site (Ding et al., 2019). However, compositional data of $PM_{2.5}$ OMMs were far less frequently used to apportion carbonaceous aerosols to sources than those of elements in Chinese cities (Tian et al., 2016; Wang et al., 2015; Wang et al., 2016; Yu et al., 2020). Studies related to gas/particle partitioning of SVOCs were limited to toxic compounds, like PAHs and their oxygen and nitrogen containing derivatives (Hu et al., 2019; Wei et al., 2015), polybrominated diphenyl ethers (Tian et al., 2011; Yang et al., 2013), and polychlorinated biphenyls (Han et al., 2010; Wu et al., 2017; Zhu et al., 2017). The influence of gas/particle partitioning on source apportionment was not ever addressed by measuring gas-phase OMMs in Chinese cities, although relatively few studies made predictions based on the equilibrium absorptive partitioning theory (Gao et al., 2015; Han et al., 2018; Wang et al., 2016).

The present study attempts to characterize gaseous and $PM_{2.5}$ nonpolar OMMs, including *n*-alkanes, PAHs, oxygenated PAHs (oxy-PAHs), hopanes, and steranes at a suburban site in northern Nanjing. Gaseous and $PM_{2.5}$ OMMs were collected using a medium volume sampler equipped with quartz fiber filters and PUF/XAD-4/PUF (PXP) adsorbent sandwich cartridges. A backup quartz filter was installed behind the front filter loaded with $PM_{2.5}$ (QBQ method) to estimate sampling artifacts due to the evaporation loss and adsorption of gas-phase OMMs. Absorptive gas/particle partitioning coefficients were calculated by definition ($K^{m}_{p,OM}$) and predicted ($K^{t}_{p,OM}$) based on the equilibrium absorptive partitioning theory (Pankow, 1994a, 1994b). Finally, total concentrations of selected OMMs covering a wide range of vapor pressures (10^{-4}–10^{-15} atm) were used as inputs for PMF analysis. The study results will benefit future field and modeling work and the development of air pollution control policy.

2. Methods

2.1. Sampling

Air samples were collected on the rooftop of the seven-story library in the Nanjing University of Information Science and Technology (NUIST 32.21°N, 118.71°E). This site was selected due to its location in a suburban residential community 20 km to the north of downtown Nanjing. The closest heavily traveled expressway is at least 1.5 km east of the sampling site. $PM_{2.5}$ and gaseous OMMs were collected using two identical medium volume samplers ($PM_{2.5}$-PUF-300) equipped with 2.5 μm cut impactors at a flow rate of 300 L min^{-1}. One of the two samplers ("Sampler I") was installed with a filter pack containing two prebaked (550°C, 4 hr) quartz filters (20.3 × 12.6 cm, Munktell Filter AB, Sweden) in series, followed by a PUF (65 mm diameter and 37.5 mm length)/XAD-4 resin (5 g)/PUF (PXP) sandwich cartridge. The other one ("Sampler II") was set up similarly using bare PUF (65 mm diameter and 37.5 mm length) instead of PXP as the sampling adsorbent. Quartz filter and PXP samples from Samplers I were used for the analysis

of nonpolar OMMs in this work. From September 28, 2018 to September 29, 2019, Sampler I was operated every sixth day during 8:00 a.m.–7:00 p.m. (daytime) and 7:00 p.m.–7:00 a.m. (next day; nighttime), and more than 100 pairs of filter and PXP samples were obtained. The top quartz filter loaded with $PM_{2.5}$ (Q_f) was used for the determination of particle-phase organics; the backup quartz filter (Q_b) was used to examine potential sampling artifacts; nonpolar OMMs detected in PXP samples were supposed to exist in the gas phase. To monitor the sampling efficiency of gaseous OMMs, breakthrough experiments were conducted during 9 sampling intervals by coupling two aforementioned PXP adsorbent sandwiches in series. Field blanks of filter and PXP media were collected every tenth sample to address potential contaminations. Prior to sampling, solid adsorbents (PUF and XAD-4) were Soxhlet extracted and dried in a same manner as Xie et al. (2014a). All filter and PXP samples were stored in prebaked glass jars under −20°C until analysis.

2.2. Chemical Analysis

Bulk OC and EC on Q_f and Q_b were determined using a thermal-optical instrument (DRI 2001A, Atmoslytic, United States) operated with the IMPROVE A protocol. Target OMMs on filter and PXP samples were extracted and analyzed using a method similar to that detailed in Xie et al. (2014a). Briefly, 1/8 (~25 cm^2) of each filter sample (Q_f and Q_b) was prespiked with 20 μL of internal standard (IS) solution containing five isotopically labeled PAHs (10 ng μL^{-1} of naphthalene-d8, acenaphthene-d10, phenanthrene-d10, chrysene-d10, and perylene-d12) and sonicated in methylene chloride twice (15 min each). After filtration and rotary evaporation, the extract was blown down to ~200 μL prior to instrumental analysis using an Agilent 7890B gas chromatography (GC) coupled to an Agilent 5977B mass spectrometer (MS). An extract volume of 2 μL was injected splitlessly and separated using an Agilent HP-5 ms capillary column (30 m × 0.25 mm × 0.25 μm). The GC oven temperature was 50°C for the first 3 min and programmed to 325°C at a ramp rate of 30°C min^{-1} (held for 10 min). GC-MS analysis of sample extracts was conducted in autosampler sequences, and the mass quantification was fulfilled by using the IS method with six-point calibration curves. PXP samples were prespiked with 20 μL of the aforementioned IS mixture at 50 ng μL^{-1} and Soxhlet extracted using 250 mL methylene chloride for 24 hr. Then the extracts were filtered and concentrated to ~1 mL for GC-MS analysis following the same method. Target OMMs and their quantification standards are listed in Table S1.

All measurements involved in this study were corrected by field blanks, and the final ambient concentrations of the measured species were calculated based on the total amount derived from instrumental analysis and sample volumes. Table S2 shows concentration statistics, including median, mean, and ranges of OMMs on Q_f, Q_b, and PXP. Recoveries of target OMMs were determined by spiking known amounts of standards to blank sampling media (quartz filter and PXP) and following the extraction and analysis procedures detailed above. As the variations of *n*-alkanes ranging from *n*-C12 to *n*-C17 in blank PXP media were mostly larger than the spiked amount (500 ng), we did not obtain reasonable recoveries for these low MW *n*-alkanes. However, the concentrations of *n*-C12 to *n*-C17 in PXP samples are at least 5 times higher than field blanks and are still included for analysis. Method detection limits (MDL) of OMMs were estimated as three times the standard deviation of their concentrations quantified from six injections of the lowest calibration standard. Table S3 provides recovery and MDL results for standard compounds. Measurement results of OMMs in filter and PXP samples were not adjusted by recoveries.

2.3. Artifact Corrections and Breakthrough Calculation

The QBQ approach was typically used to estimate positive artifacts on the bare quartz filter for long-term OC sampling (e.g., ~24 hr; Chow et al., 2010; Subramanian et al., 2004), but the filter-based sampling artifacts due to gaseous adsorption ("blow on" effect, positive artifact) and evaporation loss ("blow off" effect, negative artifact) were less considered in filed measurements of gas- and particle-phase OMMs. Xie et al. (2014a) applied the QBQ method to correct sampling artifacts of nonpolar OMMs in two different ways. One assumed that the Q_b values were totally caused by gaseous adsorption, which neglected the contribution from Q_f evaporation (C1; Table 1). The other made no correction on Q_f measurements by presuming that the adsorption artifact was offset by the evaporation loss (C2). However, none of these two methods is applicable to the condition when negative artifacts dominate OMMs concentrations on Q_b. In the current work, we developed a new method considering the changes in relative contributions of positive and negative artifacts.

Table 1
Sampling Artifact Corrections of Organic Molecular Makers (OMMs) Based on Q_b Measurements

Method	Particle phase	Gas phase	Assumptions
C1[a]	$Q_b/Q_f \geq 1$: 0	$Q_b/Q_f \geq 1$: $Q_f + Q_b$ + PXP	OMMs on Q_b are always contributed by gas-phase adsorption only
	$Q_b/Q_f < 1$: $Q_f - Q_b$	$Q_b/Q_f < 1$: PXP + $2Q_b$	
C2[a]	Q_f	PXP + Q_b	OMMs on Q_b are equally contributed by positive and negative artifacts
C3	$Q_b/Q_f \geq 1$: 0	$Q_b/Q_f \geq 1$: $Q_f + Q_b$ + PXP	$Q_b/Q_f \geq 1$: Concentrations of OMMs in Q_f and Q_b samples are completely derived from gas-phase adsorption
	$Q_b/Q_f < 1$: $Q_f - Q_b \times (Q_b/Q_f) + Q_b \times (1-Q_b/Q_f)$	$Q_b/Q_f < 1$: PXP + $2Q_b \times (Q_b/Q_f)$	$Q_b/Q_f < 1$: Q_b/Q_f is used to split the sampling artifacts estimated from Q_b measurements into positive and negative artifacts

[a]Obtained from Xie et al. (2014a).

As shown in Table 1, if the concentration ratio of a specific OMM on Q_b to Q_f is greater than unity, the specific OMM is only distributed in the gas phase and its gas-phase concentration is the sum of Q_f, Q_b, and PXP values. This situation happened to low MW *n*-alkanes (carbon number <23) and PAHs (MW < 178) mainly in summertime, which was attributed to the fact that Q_f and Q_b had different adsorption capacity, and the gaseous OMMs adsorbed on Q_f might evaporate and readsorb onto Q_b when air conditions (e.g., temperature, gaseous OMMs concentrations) changed (Hart & Pankow, 1994; Pankow & Bidleman, 1992). Xie et al. (2014a) also observed Q_b/Q_f values higher than unity for low MW OMMs in urban Denver. When $Q_b/Q_f < 1$, the Q_b/Q_f ratio will be used to split the concentrations of OMMs on Q_b into positive and negative artifacts (C3), and negative artifacts become dominant as Q_b/Q_f approaches 0. The OC detected on Q_b consisted of a mixture of mainly volatile and semivolatile organics, but not a specific OMM. Subramanian et al. (2004) demonstrated that the QBQ method could provide reasonable estimates of the positive artifact for particulate OC sampling. Here, the average concentration of OC on Q_b (0.76 ± 0.52 μg m^{-3}) was comparable to those obtained in Pittsburg, PA (0. 53 μg m^{-3}; Subramanian et al., 2004) and Denver, CO (0.48 μg m^{-3}; Xie et al., 2014a). To maintain the consistency with the previous studies, the concentrations of particulate OC were calculated by simply subtracting OC on Q_b from Q_f.

The PXP adsorbent sandwich has been demonstrated as efficient sampling media for gaseous nonpolar OMMs (Xie et al., 2014a). However, the size of PUF and height of the XAD-4 column can be different. To validate the sampling efficiency of gaseous OMMs in this work, nine pairs of front and backup PXP were collected and analyzed identically as other samples, and the breakthrough of each OMM was calculated as

$$B = \frac{[\mathrm{PXP}]_{\mathrm{back}}}{[\mathrm{PXP}]_{\mathrm{front}} + [\mathrm{PXP}]_{\mathrm{backup}}} \times 100\% \quad (1)$$

where B is the specific gas-phase breakthrough (%) and [PXP] denotes the concentration of each OMM in the front or backup PXP. For B values approaching or exceeding 50%, there will be complete breakthrough. Peters et al. (2000) set up a critical value of 33% to indicate the occurrence of excessive breakthrough. Table S4 summarizes the averages and ranges of breakthrough values for light OMMs. Other compounds with higher molecular weight (MW) were not observed in backup PXP samples.

2.4. Calculations of Absorptive Gas/Particle Partitioning Coefficients

The absorptive partitioning theory has been successively applied in explaining the gas to particle distribution of nonpolar OMMs (Liang & Pankow, 1996; Liang et al., 1997; Mader & Pankow, 2002). In this work, the absorptive gas/particle partitioning coefficient ($K_{\mathrm{p,OM}}$, m^3 μg^{-1}) was calculated empirically from

$$K^{\mathrm{m}}_{\mathrm{p,OM}} = \frac{K^{\mathrm{m}}_{\mathrm{p}}}{f_{\mathrm{OM}}} = \frac{F/M_{\mathrm{OM}}}{A} \quad (2)$$

where $K^{\mathrm{m}}_{\mathrm{p}}$ is the measured gas/particle partitioning coefficient (m^3 μg^{-1}), f_{OM} is the weight fraction of the absorptive organic matter (OM) in the total PM phase, M_{OM} is the mass concentration of particulate OM

(OC × 1.6; Turpin & Lim, 2001), and F and A are particle-phase and gas-phase concentrations of individual OMMs, respectively. Furthermore, the $K_{p,OM}$ was also predicted theoretically from

$$K^{t}_{p,OM} = \frac{RT}{10^{6}\overline{MW}_{OM}\zeta_{OM}p^{o}_{L}} \quad (3)$$

where R (m^3 atm K^{-1} mol^{-1}) and T (K) are the ideal gas constant and ambient temperature, a constant $\overline{MW}_{OM}$of 200 g mol^{-1} is assumed for the average MW of absorptive OM, ζ_{OM} is the mole fraction scale activity coefficient and presumed to be unity for all OMMs, and p^{o}_{L} is the vapor pressure (atm) of each pure compound. For each sampling interval, p^{o}_{L} values of individual OMMs were estimated from their subcooled liquid vapor pressures ($p^{o,*}_{L}$) and enthalpy of vaporization (ΔH^{*}_{vap}, kJ mol^{-1}) at 298.15 K using

$$p^{o}_{L} = p^{o,*}_{L}\exp\left[\frac{\Delta H^{*}_{vap}}{R}\left(\frac{1}{298.15}-\frac{1}{T}\right)\right] \quad (4)$$

where $p^{o,*}_{L}$ values of n-alkanes, PAHs, and oxy-PAHs were predicted using the Toxicity Estimation Software Tool (T.E.S.T) developed by the U.S. Environmental Protection Agency, while those for hopanes and steranes were obtained from Xie et al. (2013). ΔH^{*}_{vap} values were estimated from the empirical correlation between ΔH^{*}_{vap} and the logarithm of $p^{o,*}_{L}$ as follows (Goss & Schwarzenbach, 1999)

$$\Delta H^{*}_{vap} = -3.82 In p^{o,*}_{L} + 70.0 \quad (5)$$

2.5. PMF Source Apportionment

The U.S. EPA PMF version 5.0 was used as the primary source apportionment tool in this work. Besides resolving factor profiles and contributions were based on input data using a weighted least squares fitting approach, and this PMF version also developed three built-in functions (bootstrapping, displacement, and bootstrapping-displacement) for robustness assessment of the base-case solution. The assessment results have been referred to in determining the final factor number in several studies (Liu et al., 2017; Wang et al., 2017, 2018; Yu et al., 2019, 2020). In this work, a matrix of total OMMs data ($Q_f + Q_b$ + PXP) was used as input data to apportion particulate OC and EC to sources. Due to the limit of sample number ($N = 102$), measured OMMs were prescreened based on their association with specific emission sources, total percentages (<40%) of missing values and observations below detection limit (BDL), and signal to noise (concentration/uncertainty) ratios (>2). Details of the data preparation for routine PMF analysis were provided in Text S1. The final input data set ("PMF_{total}") contained 102 observations of 46 species, and the final factor number was chosen according to the interpretability and robustness of 3-facctor to 8-factor solutions. In addition, a second matrix of particle-phase OMMs (Q_f) data ("$PMF_{particle}$") were prepared and analyzed using PMF identically. PMF_{total} and $PMF_{particle}$ solutions were compared to illustrate the advantage of using total OMMs data for source apportionment.

3. Results and Discussion

3.1. General Descriptions of Measurement Results

In Table S2, the statistics of measurement results for target OMMs in Q_f, Q_b, and PXP samples were based on observed values (including BDL measurements). Total concentrations ($Q_f + Q_b$ + PXP) of individual n-alkanes, PAHs, oxy-PAHs, hopanes, and steranes are displayed using the boxplot in Figure 1. In general, the distributions of OMMs in different sampling matrices were highly dependent on species vapor pressures. For example, n-alkanes with carbon number from 12 to 19 were predominantly observed in PXP samples (Table S2). The average concentrations of n-C14–n-C25 on Q_b (0.085 ± 0.068–1.60 ± 2.14 ng m^{-3}) were more than 10% (12%–146%) of those on Q_f (0.23 ± 1.03–7.24 ± 4.84 ng m^{-3}), indicative of substantial sampling artifacts. However, the n-alkane compounds heavier than n-C25 were rarely detected in PXP samples, and their total concentrations were dominated by Q_f values. Similar to the concentration distributions of n-alkanes, the average concentrations of light PAHs (MW < 200) in PXP samples were 1–3 orders of magnitude higher than those on Q_f and Q_b (Table S2). As the MW increased, PAHs became less frequently detected in Q_b and PXP samples. Except retene, PAHs heavier than benzo[ghi]fluoranthene (BghiF, MW = 226) had significant ($p < 0.01$) higher average concentrations in Q_f than those in PXP samples. This is because retene

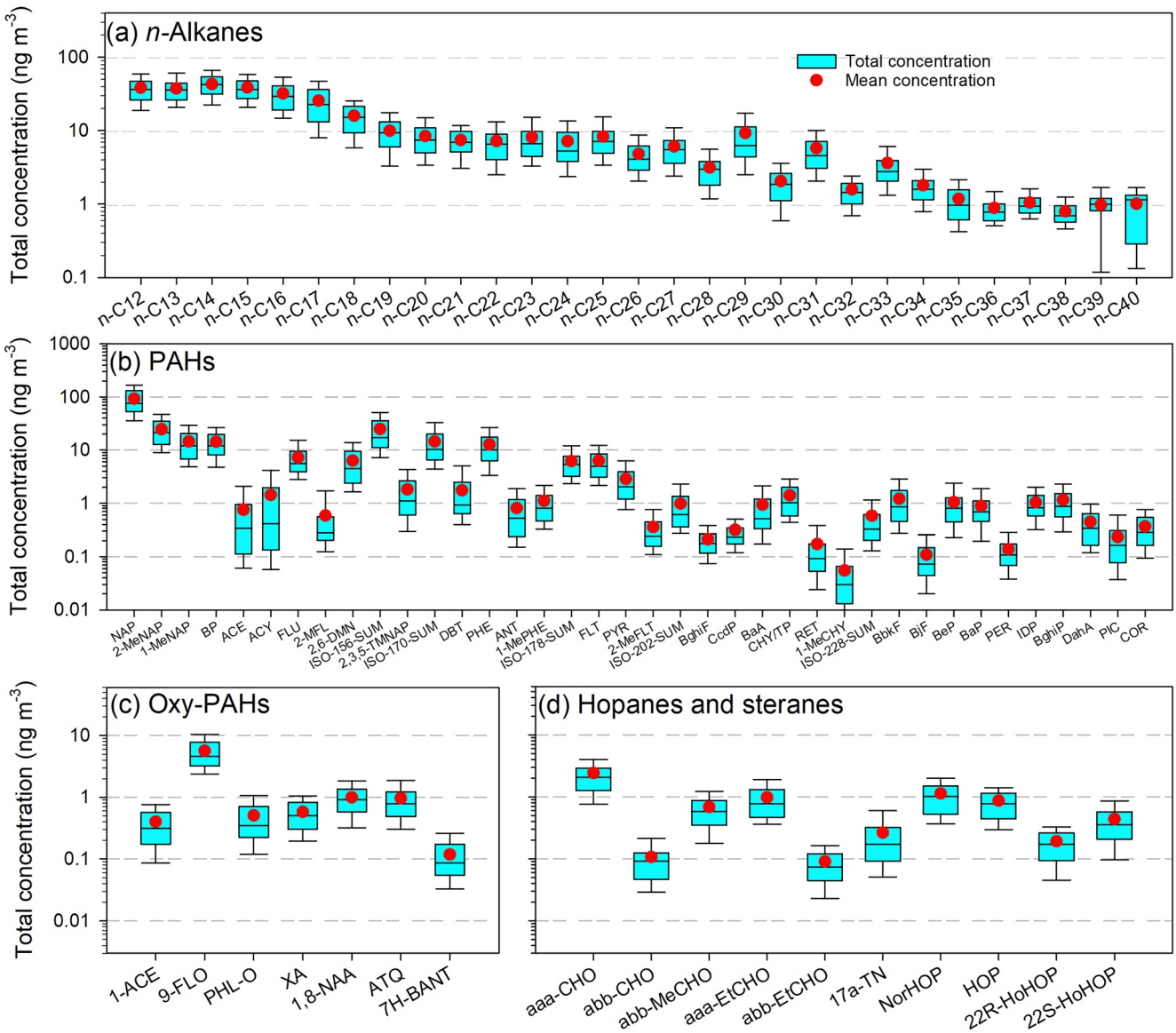

Figure 1. Total concentrations (gas + particle phases) of individual (a) *n*-alkanes, (b) polycyclic aromatic hydrocarbons (PAHs), (c) oxy-PAHs, and (d) hopanes and steranes during the sampling period. The boxes depict the median (dark line), inner quantile range (box), 10th and 90th percentiles (wishers), and the mean (red circle).

is a branched 3-ring PAH, and has greater vapor pressure (2.04×10^{-9} atm) than those lighter, but more conjugated aromatic compounds (e.g., BghiF; Table S1).

Among all oxy-PAHs species, only 1-acenaphthenone (1-ACE) and 9-fluorenone (9-FLO) were quantified in PXP samples, of which the average concentrations were significantly ($p < 0.01$) higher than those on Q_f and Q_b (Table S2). Other oxy-PAHs exhibited significant ($p < 0.01$) higher average concentrations on Q_f than those on Q_b. In Table S1, the estimated vapor pressures of 1H-phenalen-1-one (PHL-O) and xanthone (XA) are greater than that of *n*-C21, so these two compounds are expected to have substantial gas-phase concentrations. Due to the co-elution of other compounds, the chromatogram integrations of oxy-PAHs not including 1-ACE and 9-FLO in PXP samples were subject to large uncertainties and therefore not quantified here. All measured hopanes and steranes are supposed to be less volatile ($p_L^{o,*}$ 3.80×10^{-12}–2×10^{-10} atm) than *n*-C25 (3.68×10^{-10} atm; Table S1), and the nondetection in PXP samples is likely attributed to their extremely low concentrations. Total concentrations of the species not quantified in PXP samples were calculated as the sum of their Q_f and Q_b values.

In Figure 1a, low MW compounds (*n*-C12–*n*-C17) lead the total concentrations (9.98 ± 5.43–38.4 ± 17.7 ng m^{-3}) of individual *n*-alkanes. The concentration profile also shows a typical odd-to-even carbon number predominance (*n*-C27–*n*-C33) characteristic of the epicuticular wax coated on plant leaves, resembling the *n*-alkane profiles in samples of paved road dust and leaf abrasion products (Rogge et al., 1993a). Naphthalene (NAP) was the most abundant species (92.5 ± 56.7 ng m^{-3}) in measured PAHs, followed by its two methylated derivatives (2-methylnaphthalene 24.6 ± 13.7 ng m^{-3}, 1-methylnaphthalene 14.5 ± 9.29 ng m^{-3}; Figure 1b). The total concentrations of measured PAHs on Q_f were well explained by medium and high MW compounds (MW = 202–300, 81.1 ± 6.34%). When Q_b and PXP samples were included, these heavier PAHs accounted for only 8.75 ± 3.48% of the total. Unlike oxy-PAHs, hopanes and steranes had extremely low concentrations in PXP samples and were not detected. Thus, Figure 1d reflects a reliable concentration profile of hopanes and steranes in northern Nanjing. Xie et al. (2014a) measured gaseous and particle-phase nonpolar OMMs using the same sampling media at a lower flow rate of 72 L min^{-1} in urban Denver, of which the results were compared with those in this study by calculating the ratios of average total concentrations for species measured in common. As shown in Table S5, the OMMs were primarily distributed in PXP samples (e.g., light *n*-alkanes and PAHs) and the bulk OC had a smaller difference in total concentrations between northern Nanjing and urban Denver than the less volatile species and EC. The average total concentrations of several high MW PAHs (MW = 252, 276, 278) and the most abundant hopane (aaa-20R-cholestane, aaa-CHO) in this study were more than 10 times higher than those in urban Denver. Atmospheric high MW PAHs are mainly from motor vehicle emissions (Riddle et al., 2007; Rogge et al., 1993b; Schauer et al., 1996), and hopanes and steranes are commonly linked with motor oil combustions (Kleeman et al., 2008). Light *n*-alkanes and PAHs are enriched in unburned petroleum products (Li et al., 2009; Schauer et al., 1999), but they can also be emitted by a variety of combustion sources (He et al., 2010; Miguel et al., 1998; Sarti et al., 2017). Thus, the carbonaceous aerosols in northern Nanjing were more influenced by traffic exhaust emissions.

In Table S4, no species has an average breakthrough exceeding 33%, indicating efficient sampling of gaseous OMMs. However, the breakthrough values obtained in this work were much larger than those in Xie et al. (2014a). One possible explanation is that the daily average temperature during the sampling period in urban Denver (average 12.5 ± 10.1°C, range −12.6–29.4°C) was lower than (17.5 ± 9.26°C, −4.18–36.4°C) that in this study, and the lower ambient temperature would promote the retaining of gaseous OMMs on sampling adsorbent. In addition, the inner diameter (60 mm) and face velocity (1.5 cm s^{-1}) of the adsorbent cartridge in this study were larger than those (i.d. 50 mm, 0.61 cm s^{-1}) in Xie et al. (2014a). Although the same amount of XAD-4 resin (5 g) was used, the decrease in thickness of the resin bed and increased face velocity shortened the retention time of the sampled air.

3.2. Gas-Phase and Particle-Phase Separations

Gaseous and particle-phase concentrations of each OMM were calculated using three methods (C1, C2, and C3) detailed in Table 1. To simplify the comparisons across different correction methods based on Q_b measurements and the presentation of *F*% for individual OMMs, the measured species were binned into seven groups by their vapor pressures at 298.15 K ($p_L^{o,*}$, Table S6). Then total concentrations and *F*% of OMMs in each bin are illustrated in Figure 2, showing that *F*% depends negatively on species $p_L^{o,*}$. The *F*% of OMMs derived from C1, C2, and C3 corrections in the first two bins were all close to 0 ($\log p_L^{o,*} > -5$, 0.054 ± 0.064–0.083 ± 0.075%; $-6 < \log p_L^{o,*} < -5$, 0.88 ± 0.89–1.24 ± 1.01%) due to their high volatility. *F*% values in the following two bins ($-8 < \log p_L^{o,*} < -6$) calculated using methods C1 and C3 had no significant difference ($p > 0.05$). This can be attributed to the fact that OMMs in these two bins were substantially observed on Q_b and the Q_b/Q_f ratios were close to unity. Since the Q_b/Q_f ratio approached 0 when the $p_L^{o,*}$ decreased to 10^{-9} atm or below, the average *F*% calculated with method C3 ($-10 < \log p_L^{o,*} < -9$, 79.9 ± 23.5%; $\log p_L^{o,*} < -10$, 97.5 ± 3.81%) became close to C2 calculation ($-10 < \log p_L^{o,*} < -9$, 79.7 ± 19.2%; $\log p_L^{o,*} < -10$, 96.3 ± 3.79%), and were significantly ($p < 0.05$) different from the results of method C1 ($-10 < \log p_L^{o,*} < -9$, 72.2 ± 27.4%; $\log p_L^{o,*} < -10$, 93.9 ± 6.26%).

As the $p_L^{o,*}$ values of measured OMMs in this work varied by orders of magnitude, it was inappropriate to correct sampling artifacts using the same criteria for all species. For example, method C1 tended to underestimate particle-phase concentrations of medium and high MW OMMs (e.g., $\log p_L^{o,*} > -6$) due to

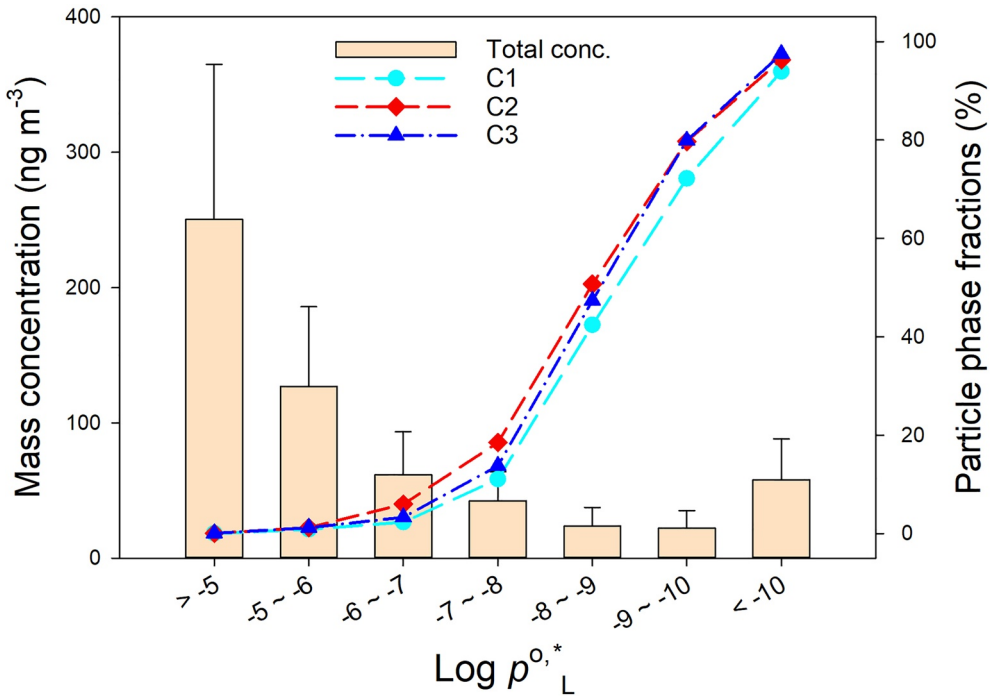

Figure 2. Total concentrations of organic molecular makers grouped by vapor pressures and their particle-phase fractions calculated based on C1, C2, and C3 corrections.

the ignorance of evaporation loss; method C2 overestimated particulate OMMs with greater volatility. As mentioned in Section 2.3, neither of these two methods considered the situation when negative artifacts dominated the contribution to OMMs on Q_b, which was applicable to high MW OMMs that were detected on Q_b but not in PXP samples. To overcome these drawbacks, method C3 was developed for the first time to separate positive and negative artifacts by utilizing the Q_b/Q_f ratio. There was no scientific evidence to support that the Q_b/Q_f was an ideal cut-off point to differentiate positive from negative artifacts, and the low and medium MW OMMs ($\log p_L^{o,*} > -9$) with significant concentrations in Q_f, Q_b, and PXP samples might have excessive evaporation loss that could not be captured by Q_b measurements.

3.3. Temporal Variations

Time series of total (gas + particle phases) and particle-phase concentrations of measured OMMs binned by their $p_L^{o,*}$ values are compared in Figure S1. Figure S2 shows temporal variations of the corresponding F% with ambient temperatures. Daytime and nighttime measurements are also distinguished in Figures S1 and S2 using different symbols. Since the filter-based measurements of OMMs were rarely corrected for sampling artifacts in previous studies, the particle-phase concentrations and F% values shown in Figures S1 and S2 were calculated using method C2 (Table 1).

In Figures S1a–S1f ($\log p_L^{o,*} > 10^{-10}$), the total concentrations of OMMs in each bin had noticeable elevations in summer periods, when particle-phase OMMs reached their minima. Only when the $p_L^{o,*}$ was lower than 10^{-10} atm, particle-phase OMMs had the same temporal pattern as that of the total OMMs (Figure S1g). These low volatile species accounted for only 10.7 ± 5.71% of the sum of total OMMs in all bins. So, barely filter-based measurements can hardly reflect the temporal variations of semivolatile OMMs in the atmosphere. As expected, F% values showed opposite trends to ambient temperatures ($r = -0.32$ to -0.88, $p < 0.01$; Figure S2). Light OMMs with $\log p_L^{o,*} > -6$ had F% values peaking on October 12, 2018 (Figure S2a), November 28, 2018, and December 23, 2018 (Figure S2b), when sudden increases in particle-phase concentrations of tetradecane (n-C14) and pentadecane (n-C15) were observed, respectively. These irregular increases are likely impacted by the coelution of other light organic compounds in the particle phase. On December 28, 2018 and December 29, 2018, F% values of OMMs with $-6 < \log p_L^{o,*} < 7$ (48.4% and

41.7%, Figure S2c) were more than five times higher than the average (6.89 ± 0.053%). This is because the ambient temperature reached its lowest level of the year (−4.2°C and −0.9°C, Figure S2), particle-phase and gas-phase OMMs had maximum and minimum concentrations, respectively (Figure S1c). Even though the average F% of the least volatile OMMs (96.3 ± 3.79%) were close to 100%, there was still an obvious dip during the hottest days in July, 2019 (Figure S2g). As mentioned in the introduction, PAHs are a group of toxic SVOCs. Their potential health risks will be underestimated if only particle-phase concentrations are taken into consideration. In this work, the benzo[a]pyrene equivalents (BaP-eq) of 18 selected PAHs were calculated using toxic equivalence factors. As shown in Figure S3, the average total BaP-eq of the 18 PAHs (2.11 ± 1.54 ng m^{-3}) are mostly accounted for by particle-phase PAHs (75.4 ± 14.2%, method C2), of which, however, the relative contributions can go down to <50% in hot periods. In Figures S1 and S2, significant diurnal variations were observed for total concentrations of OMMs only in the first four bins ($\log p_L^{o,*} > -8$). This is because these compounds primarily exist in the gas phase (Figure 2), and the gas-phase oxidation by OH radicals during the daytime is expected to be more than an order of magnitude faster than the heterogeneous oxidation (Donahue et al., 2013). The insignificant (p = 0.39–0.70) diurnal variations of heavier OMMs ($\log p_L^{o,*} < -8$) might be ascribed to the combination of influences from anthropogenic combustion emissions, atmospheric oxidations, and changes in the planetary boundary layer height.

3.4. Comparisons Between Measured and Predicted $K_{p,OM}$

In this study, the $K_{p,OM}$ values were calculated empirically ($K_{p,OM}^m$) and predicted ($K_{p,OM}^t$) using Equations 2 and 3 only for n-alkanes (n-C13–n-C34), PAHs (not including picene and coronene), and two oxy-PAHs (1-ACE and 9-FLO). Other species had very limited number of pairs of observations for gas-phase and particle-phase concentrations. The gas-phase and particle-phase data for $K_{p,OM}^m$ calculation were obtained using methods C1, C2, and C3, respectively. Figure 3 presents the average $\log K_{p,OM}^m$ of individual OMMs against their $\log p_L^{o,*}$. Also, the average $\log K_{p,OM}^t$ were linearly regressed on $\log p_L^{o,*}$ for comparison.

In Figure 3, the $\log K_{p,OM}^m$ data generally fall along the linear regression line of $\log K_{p,OM}^t$ versus $\log p_L^{o,*}$. When methods C1 and C2 were used for gas-phase and particle-phase separations, a good agreement between $\log K_{p,OM}^m$ and $\log K_{p,OM}^t$ has been observed for OMMs with $p_L^{o,*}$ ranging from 10^{-10} to 10^{-6} atm (Figures 3a, 3b, 3d and 3e). The average $\log K_{p,OM}^m$ of more volatile OMMs ($p_L^{o,*} > 10^{-6}$ atm) tended to be greater than the corresponding $\log K_{p,OM}^t$, which was attributed to the overestimation of particle-phase concentrations based on filter sampling (Xie et al., 2014a). However, the average $\log K_{p,OM}^m$ became smaller than $\log K_{p,OM}^t$ as the $p_L^{o,*}$ decreased below 10^{-10} atm. When method C3 was applied, an improved agreement between average $\log K_{p,OM}^m$ and $\log K_{p,OM}^t$ was obtained in the $p_L^{o,*}$ range of <10^{-10} atm (Figures 3c and 3f), suggesting that the evaporation loss was likely the main contributor to high MW OMMs on Q_b. Then methods C1 and C2 overestimated the gas-phase concentrations of OMM with $p_L^{o,*} < 10^{-10}$ atm. However, the average $\log K_{p,OM}^m$ values of n-C21–n-C26 for method C3 had larger deviations from $\log K_{p,OM}^t$ than those for methods C1 and C2. Thus, method C3 might be more suitable for the separation of gas-phase and particle-phase OMMs only at $p_L^{o,*} < 10^{-10}$ atm.

To understand the influence of artifact correction on the calculation of $K_{p,OM}^m$, $\log K_{p,OM}^m$ of six n-alkanes and six PAHs with $p_L^{o,*}$ varying from <10^{-10} to >10^{-5} atm were linearly regressed over their $\log K_{p,OM}^t$ for each artifact correction method (Figures S4 and S5). Due to the overestimation of particle-phase OMMs at $p_L^{o,*} > 10^{-5}$ atm, the scatter of n-C14 data clustered right above the 1:1 line for all the three artifact correction methods (Figures S4a–S4c). Only when method C2 was applied, the n-C18 scatters fell along a relatively continuous line with a significant correlation (r = 0.71, $p < 0.01$; Figures S4d–S4f). Log $K_{p,OM}^m$ values of n-C22 and n-C25 were strongly correlated with their $\log K_{p,OM}^t$ (r = 0.78–0.90, $p < 0.01$; Figures S4g–S4l), and the regression slopes are closer to unity for methods C1 and C2. But a better agreement between $\log K_{p,OM}^m$ and $\log K_{p,OM}^t$ was obtained for n-C26 and n-C27 when method C3 was utilized (Figures S4m–S4r). These results support the growing importance of evaporation loss with decreased $p_L^{o,*}$. To our knowledge, there was a relative dearth of evidence on the effect of negative artifacts of filter-based sampling on gas/particle partitioning of low volatile OMMs.

Unlike n-alkanes, no artifact correction method showed a noticeable advantage in improving the agreement between $\log K_{p,OM}^m$ and $\log K_{p,OM}^t$ for PAHs. In Figures S5a–S5f, the 1-methylnaphthalene (1-MeNAP) and

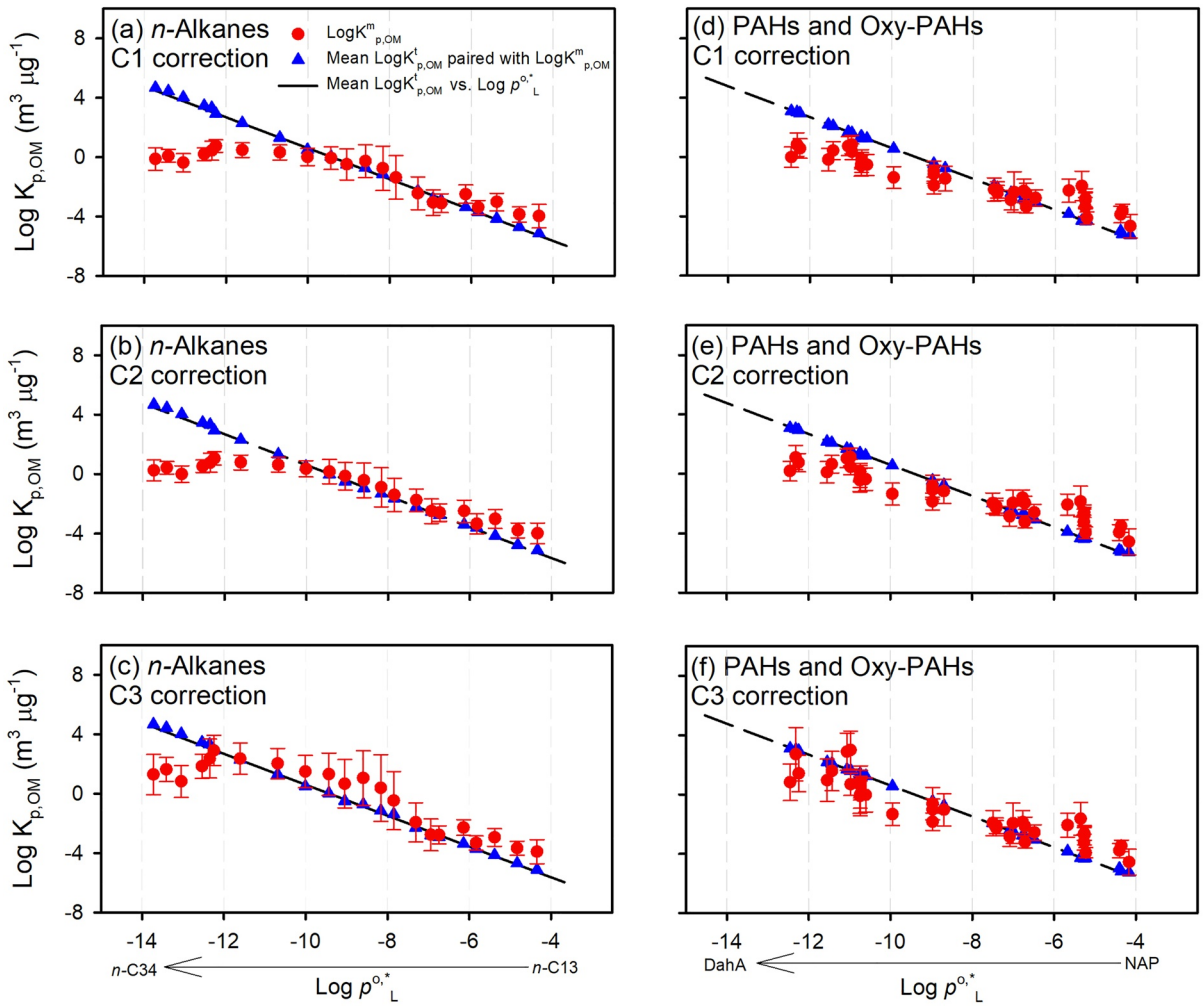

Figure 3. Comparisons of average log $K^{m}_{p,OM}$ versus log $p^{o,*}_{L}$ for (a–c) *n*-alkanes and (d–f) polycyclic aromatic hydrocarbons (PAHs)/oxy-PAHs. Particle- and gas-phase organic molecular makers are separated by using methods C1, C2, and C3, respectively. Regressions of average log $K^{t}_{p,OM}$ versus log $p^{o,*}_{L}$ are also plotted (black dashed lines), and the blue triangles represent averages of log $K^{t}_{p,OM}$ that can be paired with log $K^{m}_{p,OM}$.

2,6-dimethylnaphthalene (2,6-DMN) data gathered above the identity line. Except phenanthrene (PHE), $K^{t}_{p,OM}$ values of fluoranthene (FLT), pyrene (PYR), and benzo[a]anthracene (BaA) were more than one order of magnitude greater than their $K^{m}_{p,OM}$ (Figures S5j–S5r), which was possibly caused by the underestimation of $p^{o,*}_{L}$ using the EPA T.E.S.T tool. Figure 4 compares log $K^{m}_{p,OM}$ and log $K^{t}_{p,OM}$ of PHE, FLT, and BaA to those of *n*-alkanes with similar $p^{o,*}_{L}$ (*n*-C19, *n*-C24, and *n*-C26) in pairs. According to Equation 3, the $K^{t}_{p,OM}$ values should be the same for compounds with identical $p^{o,*}_{L}$, so the linear regressions of log $K^{t}_{p,OM}$ for the three pairs of OMMs nearly overlapped the identity line (Figure 4). However, log $K^{m}_{p,OM}$ values of PHE, FLT, and BaA were significantly ($p < 0.01$) lower than those of *n*-C19, *n*-C24, and *n*-C26, respectively, supporting the fact that PHE, FLT, and BaA should be more volatile than predicted. Furthermore, $p^{o,*}_{L}$ values of selected OMMs in this work were compared with those estimated using the group contribution methods (Hilal et al., 1995; Pankow & Asher, 2008) in Table S7. We found that the predicted $p^{o,*}_{L}$ varied by less than one order of magnitude for *n*-alkanes, but more than 1–2 orders of magnitudes for most PAHs and oxy-PAHs. Therefore, less uncertain $p^{o,*}_{L}$ values are needed to improve the prediction of $K_{p,OM}$ in future studies.

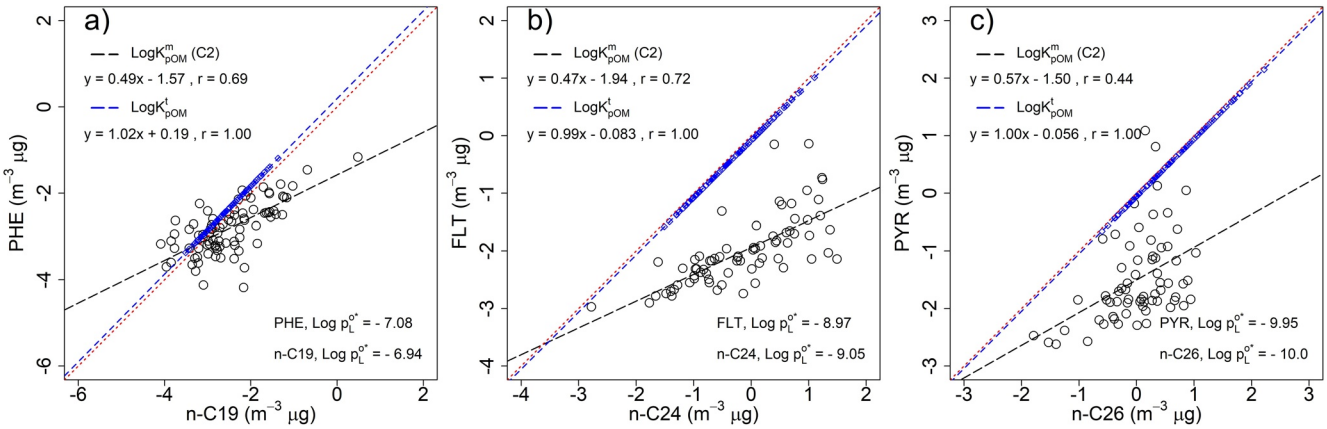

Figure 4. Scatter plots comparing $\log K^{m}_{p,OM}$, $\log K^{t}_{p,OM}$ for (a) phenanthrene (PHE) versus nonadecane (*n*-C19), (b) fluoranthene (FLT) versus tetracosane (*n*-C24), and (c) pyrene (PYR) versus hexacosane (*n*-C26).

3.5. PMF Source Apportionment

3.5.1. Overview of PMF Results

In this study, a 4-factor solution was finally determined for the PMF_{total} data set due to its most physically meaningful factors and acceptable error estimation diagnostics. Descriptions of the error estimation results for 3-factor to 8-factor solutions were provided in Text S2 and Table S8. Normalized factor profiles of the 4-factor solution in Figure 5 are calculated as

$$F^{*}_{kj} = \frac{F_{kj}}{\sum_{k=1}^{p} F_{kj}} \tag{6}$$

where F^{*}_{kj} denotes the weighting of species j in factor k relative to all other factors. Figures 6 and S6 present the contribution time series of individual factors to the sum of all input species and total OMMs, respectively, and the sum of factor contributions reproduce their concentrations very well (Figure S7). The four factors were identified as heavy *n*-alkanes, hopanes/steranes, light SVOCs, and heavy PAHs factors, and their contributions to total input species were 56.5%, 30.1%, 13.0%, and 0.53%, respectively. To illustrate the influence of gas/particle portioning of OMMs to PMF source apportionment of carbonaceous aerosols, 3-factor to 8-factor solutions were also tested for the $PMF_{particle}$ data (Text S2 and Table S9). The factor profiles and contributions of the 4-factor $PMF_{particle}$ solution are plotted on Figures 5 and 6 for comparison.

3.5.2. Interpretation of the 4-Factor PMF_{total} Solution

The heavy *n*-alkanes factor was characterized by the highest percentages of high MW *n*-alkanes (*n*-C27–*n*-C35) with a weak odd-to-even carbon number predominance (Figure 5). This *n*-alkane pattern resembled that of tire wear particles (Rogge et al., 1993a). 20%–30% of heavy PAHs (MW ≥ 252), hopanes, and steranes were also loaded on this factor, suggesting the contribution from on-road traffic. Furthermore, this factor dominated the contributions to bulk OC (60.7 ± 20.1%) and EC (55.0 ± 19.8%) and had a prominent elevation from mid-March to June (Figure 6a), when road dust tended to resuspend more frequently. Yu et al. (2020) performed the PMF analysis using hourly resolved data of elements and $PM_{2.5}$ major components (NH_4^+, SO_4^{2-}, NO_3^-, OC, and EC) from downtown Nanjing. They identified an on-road traffic factor enriched with Cu, Ba, OC, and EC, which had similar average contribution to bulk carbon contents (54.6%) and temporal variation as those of the heavy *n*-alkanes factor in this work. These results suggested that road dust resuspension should be a significant emission source for carbonaceous components in the Nanjing city. However, due to the lack of specific OMMs for secondary organic aerosol (SOA), SOA contributions were misclassified into the four resolved factors.

Hopanes and steranes are constituents of crude oil- or coal-based fuels and lubricants (Kaplan et al., 2001). These compounds are mainly contributed by coal burning, heating oil combustion, and motor vehicle emissions in ambient air (Oros & Simoneit, 2000; Rogge et al., 1993b, 1997). Besides hopanes and steranes, we

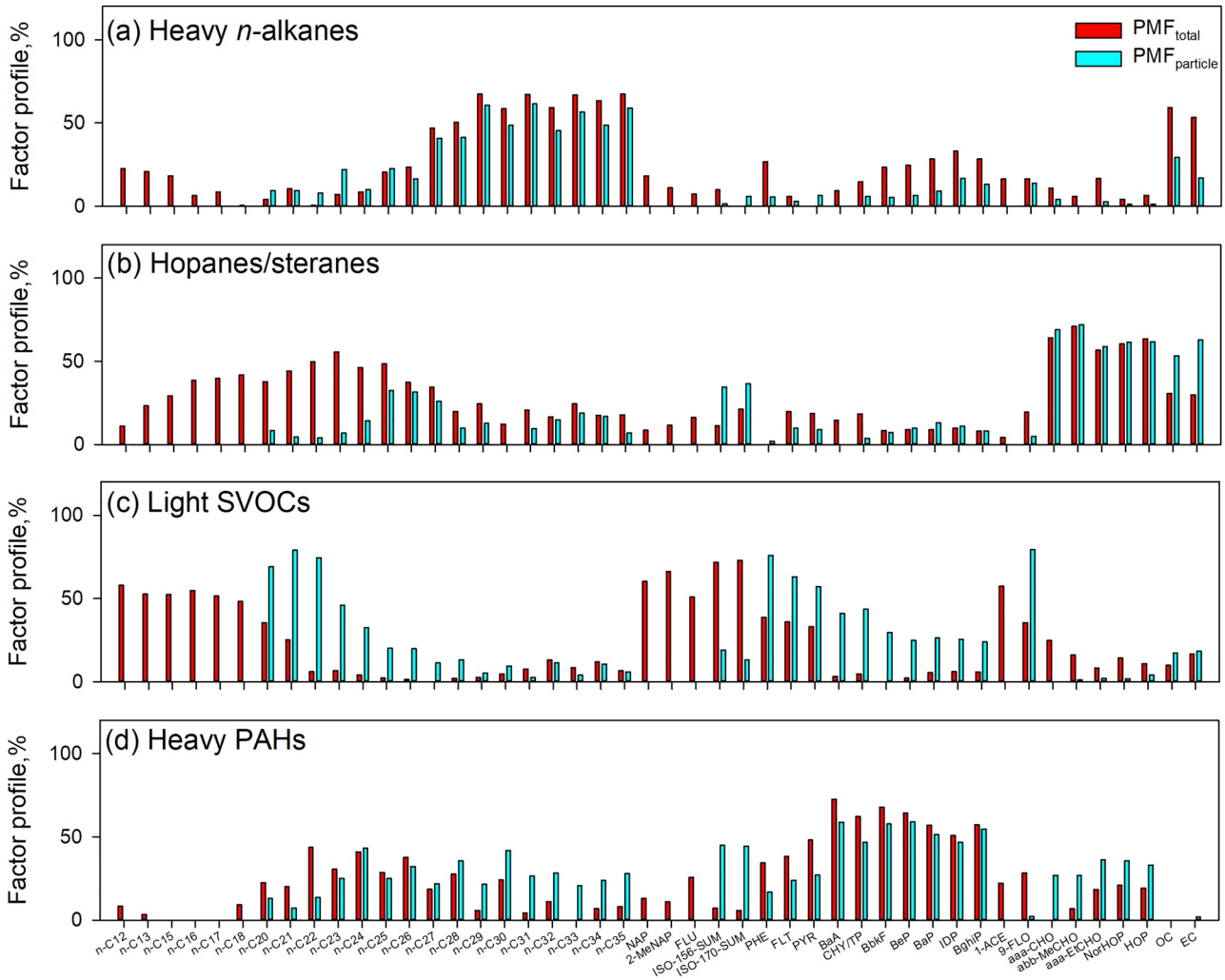

Figure 5. Comparisons of normalized factor profiles between positive matrix factorization $(PMF)_{total}$ and $PMF_{particle}$ solutions. PAHs, polycyclic aromatic hydrocarbons; SVOCs, semivolatile organic compounds.

also observe substantial *n*-alkanes with chain lengths of 13–27 peaking at *n*-C18–*n*-C25 in Figure 5b, which is consistent with the *n*-alkane profile of the engine lubricating oil (Caravaggio et al., 2007). In addition, the hopanes/steranes factor exhibited elevated contributions mainly in summer (Figure 6b). So, this factor might be linked with both combustions and evaporations of lubricants.

The light SVOCs factor consisted mainly of low MW *n*-alkanes (*n*-C12–*n*-C20), PAHs (MW = 128–202), and oxy-PAHs (1-AEC and 9-FLO). The $p_L^{o,*}$ values of these compounds are all larger than 10^{-10} atm (Table S6), explaining their increased contributions during hot periods (Figures 6c and S6c). Furthermore, the *n*-alkane and PAH patterns of the light SVOCs factor reflected the composition characteristics of crude oil and petroleum products (e.g., gasoline, diesel fuel) (Schauer et al., 1999, 2002; Wang et al., 2003), and there were large-scale petrochemical industries ~6 km to the northeast of the sampling site. Thus, the light SVOCs factor represented evaporation emissions of crude oil and petroleum products.

The heavy PAHs factor described 50.9%–72.7% of PAHs with MW ranging from 228 to 276 (Figure 5d). It also contributed significant fractions of medium *n*-alkanes (*n*-C22–*n*-C30) featured by obvious even-to-odd carbon number predominance. Unlike other factors, the heavy PAHs factor showed maximum contributions in winter (Figure 6d). In Southern China, local fossil fuel combustions and regional transport of pollutants from the north were the main cause of enhanced concentrations of PAHs during cold periods (Yan et al., 2019). So, the heavy PAHs factor was categorized as regional combustion emissions.

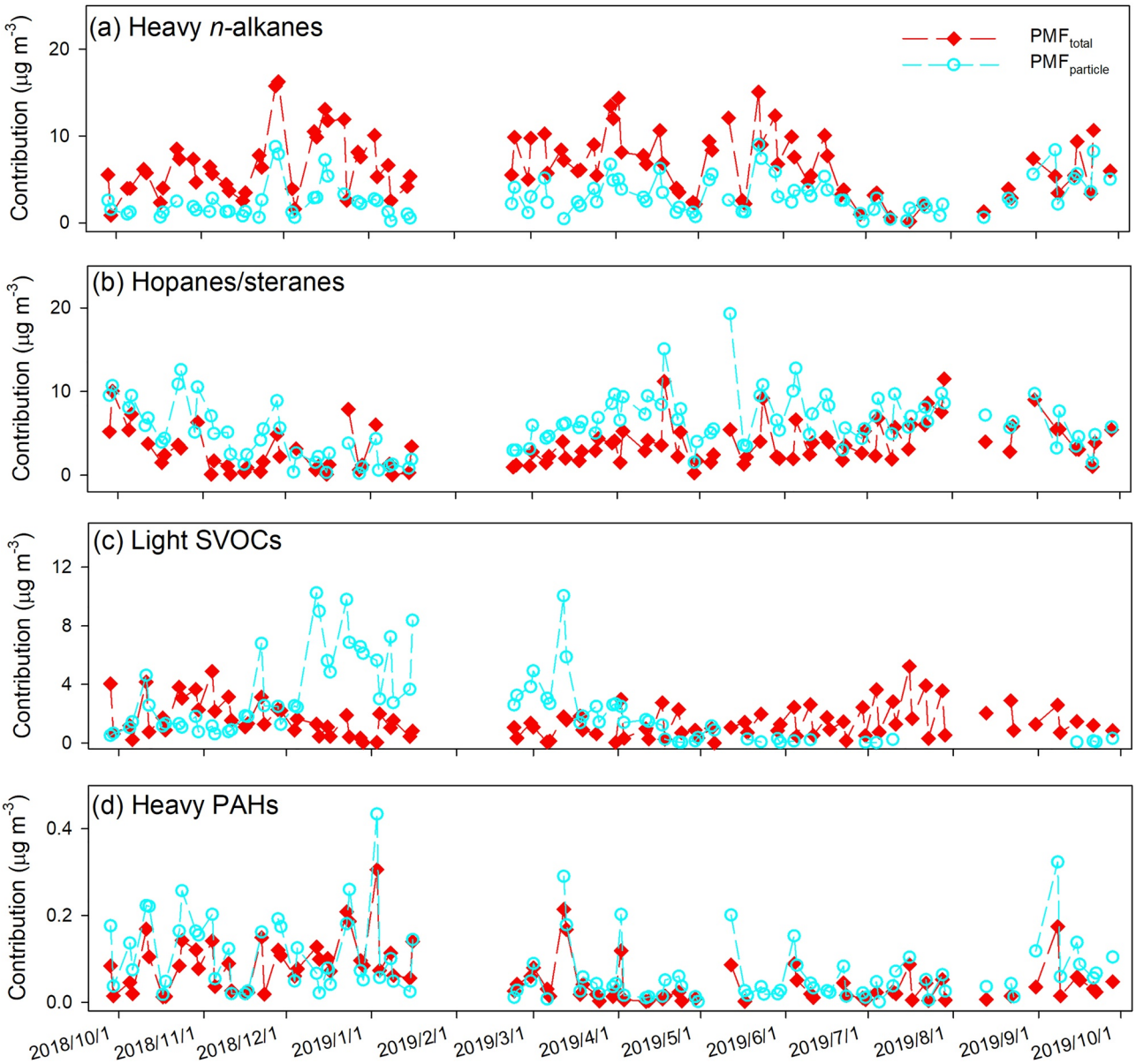

Figure 6. Time series of factor contributions to the sum of input species for positive matrix factorization $(PMF)_{total}$ and $PMF_{particle}$ solutions. PAHs, polycyclic aromatic hydrocarbons; SVOCs, semivolatile organic compounds.

3.5.3. $PMF_{particle}$ Versus PMF_{total} Solutions

Filter-based measurements of OMMs coupled to receptor modeling were well established for source apportionment of carbonaceous aerosols. The time series of species concentrations or resulting source contributions have been linked with health effects in epidemiological studies (Ito et al., 2006; Kim et al., 2012; Laden et al., 2000; Mar et al., 2005). The distinguishment of factor profiles and contributions by receptor modeling depends largely on the intersample variability of input species (Dall'Osto et al., 2013). If only particle-phase OMMs data are input for receptor modeling, the contribution time series of each output factor/source as well as its estimated health effects will be biased due to the influences of gas/particle partitioning (Xie et al., 2013, 2014b). As shown in Figure 5, each factor of the $PMF_{particle}$ solution can be uniquely matched to a PMF_{total} factor based on factor profiles, while remarkable differences were observed when comparing contribution time series of the light SVOC factor (Figures 6c and S6c). Since low MW OMMs were predominately distributed in the gas phase, the hopanes/steranes factor of the $PMF_{particle}$ solution did not have an

n-alkane pattern resembling the composition of lubricating oils (Figure 5b). The average relative contribution of the hopanes/steranes factor derived from the $PMF_{particle}$ solution (51.8%) was much greater than that from the PMF_{total} solution (30.1%). Due to the lack of gaseous OMMs data, the $PMF_{particle}$ solution over-attributed medium and high MW alkanes and PAHs to the light SVOCs factor; factor contributions of the light SVOCs factor were not correlated ($r = -0.16$, $p = 0.16$) between the $PMF_{particle}$ and PMF_{total} solutions.

Xie et al. (2013, 2014b) raised that the influence of gas/particle partitioning on PMF source apportionment could be removed by using the total OMMs data. Due to the lack of enough observations, Xie et al. (2014b) constructed $PMF_{particle}$ and PMF_{total} data sets using the same compounds, and *n*-C22 and fluoranthene (FLT) were the most volatile species among input OMMs. In this study, the involvements of low MW *n*-alkanes (*n*-C12–*n*-C21) and PAHs (MW = 128–178) accentuated the influence of gas/particle partitioning, and improved the attribution of individual factors to specific emission sources. For example, the light SVOCs factor of the $PMF_{particle}$ solution had elevated contributions only in winter, and thus could not be linked with fossil fuel evaporation; the hopanes/steranes factor from the PMF_{total} solution might not be uniquely associated with the use of lubricant oil without referring to its *n*-alkane pattern. However, the impact of other atmospheric processes like photochemical oxidations cannot be ruled out. Both high and low volatile OMMs are subject to oxidations on atmospherically relevant time scales (Lambe et al., 2009; Riva et al., 2015; Weitkamp et al., 2008), and the oxidation of OMMs in the gas phase is expected to proceed much more rapidly than that in the condensed phase (Donahue et al., 2013; Rudich et al., 2007). Saleh et al. (2013) demonstrated that the equilibration time scales of gas/particle partitioning were on orders of minutes to tens of minutes, supporting the assumption of instantaneous equilibrium employed in most chemical transport models. Then the fast gas-phase oxidation will induce evaporation of OMMs in the particle phase, accelerating the depletion of OMMs in the atmosphere. May et al. (2012) found that OMMs underwent accelerated oxidation even when only 5% of the amount was present in the gas phase. Thus, more work is warranted accounting for both gas/particle partitioning and chemical reactions in source apportionment using OMMs data.

4. Conclusions

This work investigated the ambient levels, gas/particle partitioning, and sources of nonpolar OMMs at a suburban site in northern Nanjing. Concentrations of *n*-alkanes and PAHs generally followed a decreasing trend with the increase in MW. In comparison to urban Denver, the motor vehicle exhaust had more influence on ambient levels of low-volatile or nonvolatile species in northern Nanjing. Although the particle-phase fractions of OMMs were determined by their vapor pressures, they could be biased if sampling artifacts were not appropriately corrected. Concentrations of total and particle-phase OMMs exhibited distinct temporal patterns, indicating that the total OMMs data should be used instead of the particle-phase data for the receptor-based source apportionment and health risk analysis. The comparisons of both log $K^{m}_{p,OM}$ versus log $p^{o,*}_{L}$ and log $K^{m}_{p,OM}$ versus log $K^{t}_{p,OM}$ for individual OMMs suggest that the evaporation loss is likely the main sampling artifact when $p^{o,*}_{L}$ is lower than 10^{-10} atm. To improve the prediction of absorptive gas/particle partitioning coefficients of OMMs, a more refined method for $p^{o,*}_{L}$ estimation is needed. By comparing PMF_{total} and $PMF_{particle}$ solutions, more volatile species and gas-phase OMMs data should be included for source apportionment to remove the influence of gas/particle partitioning and reduce the ambiguity of resulting factors/sources.

Conflict of Interest

The authors declare no conflicts of interest relevant to this study.

Data Availability Statement

Data used in the writing of this paper (and its supplementary information file) are publicly available on Harvard Dataverse (https://doi.org/10.7910/DVN/0GHDH4).

Acknowledgments
This research was supported by the National Natural Science Foundation of China (NSFC, 41701551), the Fundamental Research Funds for the Central Universities (KJQN202122), and Postdoctoral Research Foundation of China (2020M671519).

References

Bond, T. C., Doherty, S. J., Fahey, D. W., Forster, P. M., Berntsen, T., DeAngelo, B. J., et al. (2013). Bounding the role of black carbon in the climate system: A scientific assessment. *Journal of Geophysical Research: Atmospheres*, *118*(11), 5380–5552. https://doi.org/10.1002/jgrd.50171

Caravaggio, G. A., Charland, J.-P., Macdonald, P., & Graham, L. (2007). *n*-alkane profiles of engine lubricating oil and particulate matter by molecular sieve extraction. *Environmental Science & Technology*, *41*(10), 3697–3701. https://doi.org/10.1021/es062233h

Chow, J. C., Watson, J. G., Chen, L. W. A., Rice, J., & Frank, N. H. (2010). Quantification of $PM_{2.5}$ organic carbon sampling artifacts in US networks. *Atmospheric Chemistry and Physics*, *10*(12), 5223–5239. https://doi.org/10.5194/acp-10-5223-2010

Dall'Osto, M., Querol, X., Amato, F., Karanasiou, A., Lucarelli, F., Nava, S., et al. (2013). Hourly elemental concentrations in $PM_{2.5}$ aerosols sampled simultaneously at urban background and road site during SAPUSS—Diurnal variations and PMF receptor modelling. *Atmospheric Chemistry and Physics*, *13*(8), 4375–4392. https://doi.org/10.5194/acp-13-4375-2013

Ding, A., Huang, X., Nie, W., Chi, X., Xu, Z., Zheng, L., et al. (2019). Significant reduction of $PM_{2.5}$ in eastern China due to regional-scale emission control: Evidence from SORPES in 2011–2018. *Atmospheric Chemistry and Physics*, *19*(18), 11791–11801. https://doi.org/10.5194/acp-19-11791-2019

Donahue, N. M., Chuang, W., Epstein, S. A., Kroll, J. H., Worsnop, D. R., Robinson, A. L., et al. (2013). Why do organic aerosols exist? Understanding aerosol lifetimes using the two-dimensional volatility basis set. *Environmental Chemistry*, *10*(3), 151–157. https://doi.org/10.1071/en13022

Donahue, N. M., Robinson, A. L., Stanier, C. O., & Pandis, S. N. (2006). Coupled partitioning, dilution, and chemical aging of semivolatile organics. *Environmental Science & Technology*, *40*(8), 2635–2643. https://doi.org/10.1021/es052297c

Feng, Y., Ramanathan, V., & Kotamarthi, V. R. (2013). Brown carbon: A significant atmospheric absorber of solar radiation? *Atmospheric Chemistry and Physics*, *13*(17), 8607–8621. https://doi.org/10.5194/acp-13-8607-2013

Gao, B., Wang, X.-M., Zhao, X.-Y., Ding, X., Fu, X.-X., Zhang, Y.-L., et al. (2015). Source apportionment of atmospheric PAHs and their toxicity using PMF: Impact of gas/particle partitioning. *Atmospheric Environment*, *103*, 114–120. https://doi.org/10.1016/j.atmosenv.2014.12.006

Goss, K.-U., & Schwarzenbach, R. P. (1999). Empirical prediction of heats of vaporization and heats of adsorption of organic compounds. *Environmental Science & Technology*, *33*(19), 3390–3393. https://doi.org/10.1021/es980812j

Han, D., Fu, Q., Gao, S., Li, L., Ma, Y., Qiao, L., et al. (2018). Non-polar organic compounds in autumn and winter aerosols in a typical city of eastern China: Size distribution and impact of gas–particle partitioning on $PM_{2.5}$ source apportionment. *Atmospheric Chemistry and Physics*, *18*(13), 9375–9391. https://doi.org/10.5194/acp-18-9375-2018

Han, W., Feng, J., Gu, Z., Wu, M., Sheng, G., & Fu, J. (2010). Polychlorinated biphenyls in the atmosphere of Taizhou, a major e-waste dismantling area in China. *Journal of Environmental Sciences*, *22*(4), 589–597. https://doi.org/10.1016/s1001-0742(09)60150-9

Han, Y. M., Chen, L. W. A., Huang, R. J., Chow, J. C., Watson, J. G., Ni, H. Y., et al. (2016). Carbonaceous aerosols in megacity Xi'an, China: Implications of thermal/optical protocols comparison. *Atmospheric Environment*, *132*, 58–68. https://doi.org/10.1016/j.atmosenv.2016.02.023

Hart, K. M., & Pankow, J. F. (1994). High-volume air sampler for particle and gas sampling. 2. Use of backup filters to correct for the adsorption of gas-phase polycyclic aromatic hydrocarbons to the front filter. *Environmental Science & Technology*, *28*(4), 655–661. https://doi.org/10.1021/es00053a019

He, J., Zielinska, B., & Balasubramanian, R. (2010). Composition of semi-volatile organic compounds in the urban atmosphere of Singapore: Influence of biomass burning. *Atmospheric Chemistry and Physics*, *10*(23), 11401–11413. https://doi.org/10.5194/acp-10-11401-2010

Hilal, S. H., Karickhoff, S. W., & Carreira, L. A. (1995). A rigorous test for SPARC's chemical reactivity models: Estimation of more than 4300 ionization pKas. *Quantitative Structure-Activity Relationships*, *14*(4), 348–355. https://doi.org/10.1002/qsar.19950140405

Ho, K. F., Lee, S. C., Cao, J. J., Li, Y. S., Chow, J. C., Watson, J. G., & Fung, K. (2006). Variability of organic and elemental carbon, water soluble organic carbon, and isotopes in Hong Kong. *Atmospheric Chemistry and Physics*, *6*(12), 4569–4576. https://doi.org/10.5194/acp-6-4569-2006

Hu, H., Tian, M., Zhang, L., Yang, F., Peng, C., Chen, Y., et al. (2019). Sources and gas-particle partitioning of atmospheric parent, oxygenated, and nitrated polycyclic aromatic hydrocarbons in a humid city in southwest China. *Atmospheric Environment*, *206*, 1–10. https://doi.org/10.1016/j.atmosenv.2019.02.041

Ito, K., Christensen, W. F., Eatough, D. J., Henry, R. C., Kim, E., Laden, F., et al. (2006). PM source apportionment and health effects: 2. An investigation of intermethod variability in associations between source-apportioned fine particle mass and daily mortality in Washington, DC. *Journal of Exposure Science and Environmental Epidemiology*, *16*(4), 300–310. https://doi.org/10.1038/sj.jea.7500464

Jaeckels, J. M., Bae, M. S., & Schauer, J. J. (2007). Positive matrix factorization (PMF) analysis of molecular marker measurements to quantify the sources of organic aerosols. *Environmental Science & Technology*, *41*(16), 5763–5769. https://doi.org/10.1021/es062536b

Kaplan, I. R., Lu, S.-T., Alimi, H. M., & MacMurphey, J. (2001). Fingerprinting of high boiling hydrocarbon fuels, asphalts and lubricants. *Environmental Forensics*, *2*(3), 231–248. https://doi.org/10.1006/enfo.2001.0053

Kim, S.-Y., Peel, J. L., Hannigan, M. P., Dutton, S. J., Sheppard, L., Clark, M. L., & Vedal, S. (2012). The temporal lag structure of short-term associations of fine particulate matter chemical constituents and cardiovascular and respiratory hospitalizations. *Environmental Health Perspectives*, *120*(8), 1094–1099. https://doi.org/10.1289/ehp.1104721

Kleeman, M. J., Riddle, S. G., Robert, M. A., & Jakober, C. A. (2008). Lubricating oil and fuel contributions to particulate matter emissions from light-duty gasoline and heavy-duty diesel vehicles. *Environmental Science & Technology*, *42*(1), 235–242. https://doi.org/10.1021/es071054c

Laden, F., Neas, L. M., Dockery, D. W., & Schwartz, J. (2000). Association of fine particulate matter from different sources with daily mortality in six U.S. cities. *Environmental Health Perspectives*, *108*(10), 941–947. https://doi.org/10.1289/ehp.00108941

Lambe, A. T., Miracolo, M. A., Hennigan, C. J., Robinson, A. L., & Donahue, N. M. (2009). Effective rate constants and uptake coefficients for the reactions of organic molecular markers (*n*-alkanes, hopanes, and steranes) in motor oil and diesel primary organic aerosols with hydroxyl radicals. *Environmental Science & Technology*, *43*(23), 8794–8800. https://doi.org/10.1021/es901745h

Li, H., Wang, Q. G., Yang, M., Li, F., Wang, J., Sun, Y., et al. (2016). Chemical characterization and source apportionment of $PM_{2.5}$ aerosols in a megacity of Southeast China. *Atmospheric Research*, *181*, 288–299. https://doi.org/10.1016/j.atmosres.2016.07.005

Li, Z., Porter, E. N., Sjödin, A., Needham, L. L., Lee, S., Russell, A. G., & Mulholland, J. A. (2009). Characterization of $PM_{2.5}$-bound polycyclic aromatic hydrocarbons in Atlanta—Seasonal variations at urban, suburban, and rural ambient air monitoring sites. *Atmospheric Environment*, *43*(27), 4187–4193. https://doi.org/10.1016/j.atmosenv.2009.05.031

Liang, C., & Pankow, J. F. (1996). Gas/particle partitioning of organic compounds to environmental tobacco smoke: Partition coefficient measurements by desorption and comparison to urban particulate material. *Environmental Science & Technology*, *30*(9), 2800–2805. https://doi.org/10.1021/es960050x

Liang, C., Pankow, J. F., Odum, J. R., & Seinfeld, J. H. (1997). Gas/particle partitioning of semivolatile organic compounds to model inorganic, organic, and ambient smog aerosols. *Environmental Science & Technology*, *31*(11), 3086–3092. https://doi.org/10.1021/es9702529

Liu, B., Wu, J., Zhang, J., Wang, L., Yang, J., Liang, D., et al. (2017). Characterization and source apportionment of $PM_{2.5}$ based on error estimation from EPA PMF 5.0 model at a medium city in China. *Environmental Pollution*, *222*, 10–22. https://doi.org/10.1016/j.envpol.2017.01.005

Mader, B. T., & Pankow, J. F. (2002). Study of the effects of particle-phase carbon on the gas/particle partitioning of semivolatile organic compounds in the atmosphere using controlled field experiments. *Environmental Science & Technology*, *36*(23), 5218–5228. https://doi.org/10.1021/es011048v

Mar, T. F., Ito, K., Koenig, J. Q., Larson, T. V., Eatough, D. J., Henry, R. C., et al. (2005). PM source apportionment and health effects. 3. Investigation of inter-method variations in associations between estimated source contributions of $PM_{2.5}$ and daily mortality in Phoenix, AZ. *Journal of Exposure Science and Environmental Epidemiology*, *16*(4), 311–320. https://doi.org/10.1038/sj.jea.7500465

May, A. A., Saleh, R., Hennigan, C. J., Donahue, N. M., & Robinson, A. L. (2012). Volatility of organic molecular markers used for source apportionment analysis: Measurements and implications for atmospheric lifetime. *Environmental Science & Technology*, *46*(22), 12435–12444. https://doi.org/10.1021/es302276t

Miguel, A. H., Kirchstetter, T. W., Harley, R. A., & Hering, S. V. (1998). On-road emissions of particulate polycyclic aromatic hydrocarbons and black carbon from gasoline and diesel vehicles. *Environmental Science & Technology*, *32*(4), 450–455. https://doi.org/10.1021/es970566w

O'Dowd, C. D., Aalto, P., Hmeri, K., Kulmala, M., & Hoffmann, T. (2002). Atmospheric particles from organic vapours. *Nature*, *416*(6880), 497–498. https://doi.org/10.1038/416497a

Oros, D. R., & Simoneit, B. R. T. (2000). Identification and emission rates of molecular tracers in coal smoke particulate matter. *Fuel*, *79*(5), 515–536. https://doi.org/10.1016/s0016-2361(99)00153-2

Pankow, J. F. (1994a). An absorption model of gas/particle partitioning of organic compounds in the atmosphere. *Atmospheric Environment*, *28*(2), 185–188. https://doi.org/10.1016/1352-2310(94)90093-0

Pankow, J. F. (1994b). An absorption model of the gas/aerosol partitioning involved in the formation of secondary organic aerosol. *Atmospheric Environment*, *28*(2), 189–193. https://doi.org/10.1016/1352-2310(94)90094-9

Pankow, J. F., & Asher, W. E. (2008). SIMPOL.1: A simple group contribution method for predicting vapor pressures and enthalpies of vaporization of multifunctional organic compounds. *Atmospheric Chemistry and Physics*, *8*(10), 2773–2796. https://doi.org/10.5194/acp-8-2773-2008

Pankow, J. F., & Bidleman, T. F. (1992). Interdependence of the slopes and intercepts from log-log correlations of measured gas-particle paritioning and vapor pressure—I. theory and analysis of available data. *Atmospheric Environment, Part A. General Topics*, *26*(6), 1071–1080. https://doi.org/10.1016/0960-1686(92)90039-n

Peters, A. J., Lane, D. A., Gundel, L. A., Northcott, G. L., & Jones, K. C. (2000). A comparison of high volume and diffusion denuder samplers for measuring semivolatile organic compounds in the atmosphere. *Environmental Science & Technology*, *34*(23), 5001–5006. https://doi.org/10.1021/es000056t

Petters, M. D., Prenni, A. J., Kreidenweis, S. M., DeMott, P. J., Matsunaga, A., Lim, Y. B., & Ziemann, P. J. (2006). Chemical aging and the hydrophobic-to-hydrophilic conversion of carbonaceous aerosol. *Geophysical Research Letters*, *33*(24). https://doi.org/10.1029/2006GL027249

Ramírez, N., Cuadras, A., Rovira, E., Marcé Rosa, M., & Borrull, F. (2011). Risk assessment related to atmospheric polycyclic aromatic hydrocarbons in gas and particle phases near industrial sites. *Environmental Health Perspectives*, *119*(8), 1110–1116. https://doi.org/10.1289/ehp.1002855

Ravindra, Mittal, A. K., & Grieken, R. V. (2001). Health risk assessment of urban suspended particulate matter with special reference to polycyclic aromatic hydrocarbons: A review. *Reviews on Environmental Health*, *16*(3), 169–190. https://doi.org/10.1515/reveh.2001.16.3.169

Riddle, S. G., Jakober, C. A., Robert, M. A., Cahill, T. M., Charles, M. J., & Kleeman, M. J. (2007). Large PAHs detected in fine particulate matter emitted from light-duty gasoline vehicles. *Atmospheric Environment*, *41*(38), 8658–8668. https://doi.org/10.1016/j.atmosenv.2007.07.023

Riva, M., Robinson, E. S., Perraudin, E., Donahue, N. M., & Villenave, E. (2015). Photochemical aging of secondary organic aerosols generated from the photooxidation of polycyclic aromatic hydrocarbons in the gas-phase. *Environmental Science & Technology*, *49*(9), 5407–5416. https://doi.org/10.1021/acs.est.5b00442

Rogge, W. F., Hildemann, L. M., Mazurek, M. A., Cass, G. R., & Simoneit, B. R. T. (1993a). Sources of fine organic aerosol. 3. Road dust, tire debris, and organometallic brake lining dust—Roads as sources and sinks. *Environmental Science & Technology*, *27*(9), 1892–1904. https://doi.org/10.1021/es00046a019

Rogge, W. F., Hildemann, L. M., Mazurek, M. A., Cass, G. R., & Simoneit, B. R. T. (1993b). Sources of fine organic aerosol. 2. Noncatalyst and catalyst-equipped automobiles and heavy-duty diesel trucks. *Environmental Science & Technology*, *27*(4), 636–651. https://doi.org/10.1021/es00041a007

Rogge, W. F., Hildemann, L. M., Mazurek, M. A., Cass, G. R., & Simoneit, B. R. T. (1997). Sources of fine organic aerosol. 8. Boilers burning No. 2 distillate fuel oil. *Environmental Science & Technology*, *31*(10), 2731–2737. https://doi.org/10.1021/es9609563

Rudich, Y., Donahue, N. M., & Mentel, T. F. (2007). Aging of organic aerosol: Bridging the gap between laboratory and field studies. *Annual Review of Physical Chemistry*, *58*(1), 321–352. https://doi.org/10.1146/annurev.physchem.58.032806.104432

Saleh, R., Donahue, N. M., & Robinson, A. L. (2013). Time scales for gas-particle partitioning equilibration of secondary organic aerosol formed from alpha-pinene ozonolysis. *Environmental Science & Technology*, *47*(11), 5588–5594. https://doi.org/10.1021/es400078d

Sarti, E., Pasti, L., Scaroni, I., Casali, P., Cavazzini, A., & Rossi, M. (2017). Determination of n-alkanes, PAHs and nitro-PAHs in $PM_{2.5}$ and PM_1 sampled in the surroundings of a municipal waste incinerator. *Atmospheric Environment*, *149*, 12–23. https://doi.org/10.1016/j.atmosenv.2016.11.016

Schauer, J. J., Kleeman, M. J., Cass, G. R., & Simoneit, B. R. T. (1999). Measurement of emissions from air pollution sources. 2. C-1 through C-30 organic compounds from medium duty diesel trucks. *Environmental Science & Technology*, *33*(10), 1578–1587. https://doi.org/10.1021/es980081n

Schauer, J. J., Kleeman, M. J., Cass, G. R., & Simoneit, B. R. T. (2002). Measurement of emissions from air pollution sources. 5. C-1-C-32 organic compounds from gasoline-powered motor vehicles. *Environmental Science & Technology*, *36*(6), 1169–1180. https://doi.org/10.1021/es0108077

Schauer, J. J., Rogge, W. F., Hildemann, L. M., Mazurek, M. A., Cass, G. R., & Simoneit, B. R. T. (1996). Source apportionment of airborne particulate matter using organic compounds as tracers. *Atmospheric Environment*, *30*(22), 3837–3855. https://doi.org/10.1016/1352-2310(96)00085-4

Shrivastava, M. K., Subramanian, R., Rogge, W. F., & Robinson, A. L. (2007). Sources of organic aerosol: Positive matrix factorization of molecular marker data and comparison of results from different source apportionment models. *Atmospheric Environment*, *41*(40), 9353–9369. https://doi.org/10.1016/j.atmosenv.2007.09.016

Subramanian, R., Khlystov, A. Y., Cabada, J. C., & Robinson, A. L. (2004). Positive and negative artifacts in particulate organic carbon measurements with denuded and undenuded sampler configurations special issue of aerosol science and technology on findings from the fine particulate matter supersites program. *Aerosol Science and Technology*, *38*(Suppl. 1), 27–48. https://doi.org/10.1080/02786820390229354

Tian, M., Chen, S.-J., Wang, J., Zheng, X.-B., Luo, X.-J., & Mai, B.-X. (2011). Brominated flame retardants in the atmosphere of e-waste and rural sites in Southern China: Seasonal variation, temperature dependence, and gas-particle partitioning. *Environmental Science & Technology*, *45*(20), 8819–8825. https://doi.org/10.1021/es202284p

Tian, S. L., Pan, Y. P., & Wang, Y. S. (2016). Size-resolved source apportionment of particulate matter in urban Beijing during haze and non-haze episodes. *Atmospheric Chemistry and Physics*, *16*(1), 1–19. https://doi.org/10.5194/acp-16-1-2016

Tuccella, P., Curci, G., Pitari, G., Lee, S., & Jo, D. S. (2020). Direct radiative effect of absorbing aerosols: Sensitivity to mixing state, brown carbon, and soil dust refractive index and shape. *Journal of Geophysical Research: Atmospheres*, *125*(2), e2019JD030967. https://doi.org/10.1029/2019JD030967

Turpin, B. J., & Lim, H.-J. (2001). Species contributions to $PM_{2.5}$ mass concentrations: Revisiting common assumptions for estimating organic mass. *Aerosol Science and Technology*, *35*(1), 602–610. https://doi.org/10.1080/02786820119445

Wang, Q., Feng, Y., Huang, X. H. H., Griffith, S. M., Zhang, T., Zhang, Q., et al. (2016). Nonpolar organic compounds as $PM_{2.5}$ source tracers: Investigation of their sources and degradation in the Pearl River Delta, China. *Journal of Geophysical Research: Atmospheres*, *121*(19), 11862–11879. https://doi.org/10.1002/2016JD025315

Wang, Q., He, X., Huang, X. H., Griffith, S. M., Feng, Y., Zhang, T., et al. (2017). Impact of secondary organic aerosol tracers on tracer-based source apportionment of organic carbon and $PM_{2.5}$: A case study in the Pearl River Delta, China. *ACS Earth and Space Chemistry*, *1*(9), 562–571. https://doi.org/10.1021/acsearthspacechem.7b00088

Wang, Q., Qiao, L., Zhou, M., Zhu, S., Griffith, S., Li, L., & Yu, J. Z. (2018). Source apportionment of $PM_{2.5}$ using hourly measurements of elemental tracers and major constituents in an urban environment: Investigation of time-resolution influence. *Journal of Geophysical Research: Atmospheres*, *123*(10), 5284–5300. https://doi.org/10.1029/2017JD027877

Wang, Q. Q., Huang, X. H. H., Zhang, T., Zhang, Q., Feng, Y., Yuan, Z., et al. (2015). Organic tracer-based source analysis of $PM_{2.5}$ organic and elemental carbon: A case study at Dongguan in the Pearl River Delta, China. *Atmospheric Environment*, *118*, 164–175. https://doi.org/10.1016/j.atmosenv.2015.07.033

Wang, X., Heald, C. L., Ridley, D. A., Schwarz, J. P., Spackman, J. R., Perring, A. E., et al. (2014). Exploiting simultaneous observational constraints on mass and absorption to estimate the global direct radiative forcing of black carbon and brown carbon. *Atmospheric Chemistry and Physics*, *14*(20), 10989–11010. https://doi.org/10.5194/acp-14-10989-2014

Wang, Y., Li, W., Gao, W., Liu, Z., Tian, S., Shen, R., et al. (2019). Trends in particulate matter and its chemical compositions in China from 2013–2017. *Science China Earth Sciences*, *62*(12), 1857–1871. https://doi.org/10.1007/s11430-018-9373-1

Wang, Z., Hollebone, B., Fingas, M., Fieldhouse, B., Sigouin, L., Landriault, M., et al. (2003). *Characteristics of spilled oils, fuels, and petroleum products: 1. Composition and properties of selected oils*. United States Environmental Protection Agency.

Wei, C., Han, Y., Bandowe, B. A. M., Cao, J., Huang, R.-J., Ni, H., et al. (2015). Occurrence, gas/particle partitioning and carcinogenic risk of polycyclic aromatic hydrocarbons and their oxygen and nitrogen containing derivatives in Xi'an, central China. *Science of the Total Environment*, *505*, 814–822. https://doi.org/10.1016/j.scitotenv.2014.10.054

Weitkamp, E. A., Lambe, A. T., Donahue, N. M., & Robinson, A. L. (2008). Laboratory measurements of the heterogeneous oxidation of condensed-phase organic molecular makers for motor vehicle exhaust. *Environmental Science & Technology*, *42*(21), 7950–7956. https://doi.org/10.1021/es800745x

World Health Organization. (2012). *Health effects of black carbon*. WHO. Retrieved from http://www.unece.org/fileadmin/DAM/env/documents/2012/air/Health_Effects_of_Black_Carbon_report.pdf

Wu, Z., Lin, T., Li, Z., Li, Y., Guo, T., & Guo, Z. (2017). Atmospheric occurrence, transport and gas–particle partitioning of polychlorinated biphenyls over the northwestern Pacific Ocean. *Atmospheric Environment*, *167*, 487–495. https://doi.org/10.1016/j.atmosenv.2017.08.056

Xie, M., Barsanti, K. C., Hannigan, M. P., Dutton, S. J., & Vedal, S. (2013). Positive matrix factorization of $PM_{2.5}$—Eliminating the effects of gas/particle partitioning of semivolatile organic compounds. *Atmospheric Chemistry and Physics*, *13*(15), 7381–7393. https://doi.org/10.5194/acp-13-7381-2013

Xie, M., Hannigan, M. P., & Barsanti, K. C. (2014a). Gas/particle partitioning of *n*-alkanes, PAHs and oxygenated PAHs in urban Denver. *Atmospheric Environment*, *95*(0), 355–362. https://doi.org/10.1016/j.atmosenv.2014.06.056

Xie, M., Hannigan, M. P., & Barsanti, K. C. (2014b). Impact of gas/particle partitioning of semivolatile organic compounds on source apportionment with positive matrix factorization. *Environmental Science & Technology*, *48*(16), 9053–9060. https://doi.org/10.1021/es5022262

Xie, M., Hannigan, M. P., Dutton, S. J., Milford, J. B., Hemann, J. G., Miller, S. L., et al. (2012). Positive matrix factorization of $PM_{2.5}$: Comparison and implications of using different speciation data sets. *Environmental Science & Technology*, *46*(21), 11962–11970. https://doi.org/10.1021/es302358g

Yan, D., Wu, S., Zhou, S., Tong, G., Li, F., Wang, Y., & Li, B. (2019). Characteristics, sources and health risk assessment of airborne particulate PAHs in Chinese cities: A review. *Environmental Pollution*, *248*, 804–814. https://doi.org/10.1016/j.envpol.2019.02.068

Yang, M., Howell, S. G., Zhuang, J., & Huebert, B. J. (2009). Attribution of aerosol light absorption to black carbon, brown carbon, and dust in China—Interpretations of atmospheric measurements during EAST-AIRE. *Atmospheric Chemistry and Physics*, *9*(6), 2035–2050. https://doi.org/10.5194/acp-9-2035-2009

Yang, M., Qi, H., Jia, H.-L., Ren, N.-Q., Ding, Y.-S., Ma, W.-L., et al. (2013). Polybrominated diphenyl ethers in air across China: Levels, compositions, and gas-particle partitioning. *Environmental Science & Technology*, *47*(15), 8978–8984. https://doi.org/10.1021/es4022409

Yu, Y., Ding, F., Mu, Y., Xie, M., & Wang, Q. G. (2020). High time-resolved $PM_{2.5}$ composition and sources at an urban site in Yangtze River Delta, China after the implementation of the APPCAP. *Chemosphere*, *261*, 127746. https://doi.org/10.1016/j.chemosphere.2020.127746

Yu, Y., He, S., Wu, X., Zhang, C., Yao, Y., Liao, H., et al. (2019). $PM_{2.5}$ elements at an urban site in Yangtze River Delta, China: High time-resolved measurement and the application in source apportionment. *Environmental Pollution*, *253*, 1089–1099. https://doi.org/10.1016/j.envpol.2019.07.096

Zhu, Q., Zheng, M., Liu, G., Zhang, X., Dong, S., Gao, L., & Liang, Y. (2017). Particle size distribution and gas-particle partitioning of polychlorinated biphenyls in the atmosphere in Beijing, China. *Environmental Science and Pollution Research*, *24*(2), 1389–1396. https://doi.org/10.1007/s11356-016-7936-y

References From the Supporting Information

Dutton, S. J., Vedal, S., Piedrahita, R., Milford, J. B., Miller, S. L., & Hannigan, M. P. (2010). Source apportionment using positive matrix factorization on daily measurements of inorganic and organic speciated $PM_{2.5}$. *Atmospheric Environment*, *44*(23), 2731–2741. https://doi.org/10.1016/j.atmosenv.2010.04.038

Polissar, A. V., Hopke, P. K., Paatero, P., Malm, W. C., & Sisler, J. F. (1998). Atmospheric aerosol over Alaska—2. Elemental composition and sources. *Journal of Geophysical Research*, *103*(D15), 19045–19057. https://doi.org/10.1029/98JD01212

Ramírez, N., Cuadras, A., Rovira, E., Marcé Rosa, M., & Borrull, F. (2011). Risk assessment related to atmospheric polycyclic aromatic hydrocarbons in gas and particle phases near industrial sites. *Environmental Health Perspectives*, *119*(8), 1110–1116. https://doi.org/10.1289/ehp.1002855

Shrivastava, M. K., Subramanian, R., Rogge, W. F., & Robinson, A. L. (2007). Sources of organic aerosol: Positive matrix factorization of molecular marker data and comparison of results from different source apportionment models. *Atmospheric Environment*, *41*(40), 9353–9369. https://doi.org/10.1016/j.atmosenv.2007.09.016

Xie, M., Hannigan, M. P., & Barsanti, K. C. (2014). Gas/particle partitioning of *n*-alkanes, PAHs and oxygenated PAHs in urban Denver. *Atmospheric Environment*, *95*(0), 355–362. https://doi.org/10.1016/j.atmosenv.2014.06.056

Xie, M., Hannigan, M. P., Dutton, S. J., Milford, J. B., Hemann, J. G., Miller, S. L., et al. (2012). Positive matrix factorization of $PM_{2.5}$: Comparison and implications of using different speciation data sets. *Environmental Science & Technology*, *46*(21), 11962–11970. https://doi.org/10.1021/es302358g

Xie, M., Piedrahita, R., Dutton, S. J., Milford, J. B., Hemann, J. G., Peel, J. L., et al. (2013). Positive matrix factorization of a 32-month series of daily $PM_{2.5}$ speciation data with incorporation of temperature stratification. *Atmospheric Environment*, *65*(0), 11–20. https://doi.org/10.1016/j.atmosenv.2012.09.034

Yang, L., Shang, Y., Hannigan, M. P., Zhu, R., Wang, Q. G., Qin, C., & Xie, M. (2021). Collocated speciation of $PM_{2.5}$ using tandem quartz filters in northern Nanjing, China: Sampling artifacts and measurement uncertainty. *Atmospheric Environment*, *246*, 118066. https://doi.org/10.1016/j.atmosenv.2020.118066